PHYSICAL REVIEW D **95,** 094013 (2017)

Nuclear parton density functions from jet production in DIS at an EIC

M. Klasen,[*] K. Kovařík,[†] and J. Potthoff[‡]

Institut für Theoretische Physik, Westfälische Wilhelms-Universität Münster, Wilhelm-Klemm-Straße 9, D-48149 Münster, Germany

(Received 10 March 2017; published 22 May 2017)

We investigate the potential of inclusive-jet production in deep-inelastic scattering (DIS) at a future electron-ion collider (EIC) to improve our current knowledge of nuclear parton density functions (PDFs). We demonstrate that the kinematic reach is extended similarly to inclusive DIS, but that the uncertainty of the nuclear PDFs, in particular of the gluon density at low Bjorken-x, is considerably reduced, by up to an order of magnitude compared to the present situation. Using an approximate next-to-next-to-leading order (aNNLO) calculation implemented in the program `JetViP`, we also make predictions for three different EIC designs and for four different light and heavy nuclei.

DOI: 10.1103/PhysRevD.95.094013

I. INTRODUCTION

Parton density functions (PDFs) are important fundamental quantities describing our current knowledge of (primarily longitudinal) momentum distributions of quarks and gluons in protons (p) and nuclei (A). As intrinsically nonperturbative quantities, they are usually extracted by fitting perturbatively calculated cross sections, in particular of inclusive deep-inelastic scattering (DIS) in ep or eA collisions and the Drell-Yan (DY) process in pp or pA collisions, to experimental data. The predictive power of this procedure lies in the universality, i.e. the process independence of the PDFs guaranteed by the QCD factorization theorem [1] and their perturbative evolution with the resolution scale Q^2, which is typically the virtuality of the exchanged vector boson. For proton PDFs, the DESY HERA ep collider delivered an unprecedented wealth of data, which now allows for precise theoretical predictions of CERN LHC cross sections, required notably for the searches for physics beyond the Standard Model [2].

In contrast, nuclear PDFs lag considerably behind. DIS (and DY) data so far only exist in fixed-target kinematics, which considerably restricts their range in Bjorken-x and Q^2, and only with limited statistics for various nuclei (typically He, C, Ca, Fe, W, Au and Pb), often as ratios to eD or pp data. A future electron-ion collider (EIC) would therefore have a strong impact, in particular on understanding the small- and large-x regions of nuclear shadowing and the European Muon Collaboration (EMC) effect, respectively, and on pinning down the poorly restricted gluon densities in nuclei, as laid out in detail in the EIC white paper [3] and also discussed at the recent POETIC 7 conference [4]. Current analyses of nuclear PDFs like DSSZ [5] and nCTEQ15 [6] have mostly relied on inclusive pion data from the BNL RHIC to restrict the nuclear gluon PDF with the disadvantage that these data depend also on the pion fragmentation function, which may furthermore be modified by medium effects [5]. The importance of nuclear PDFs thus also lies in the fact that their knowledge is mandatory for a clean separation of cold and hot nuclear effects in the determination of the properties of the quark gluon plasma. In addition to inclusive pion data in D-Au collisions at BNL RHIC, the EPPS16 update to the EPS09 analysis uses also LHC p-Pb data on inclusive dijet production [7,8], while the update of the HKN07 analysis has focused on neutrino data [9] and the question of universality of neutral and charged current DIS [10]. Vector boson and (slightly virtual) photon production have also been suggested [11] and employed [12] as possible improvements.

In this paper, we study the impact of inclusive-jet measurements in DIS at a future EIC on the determination of nuclear PDFs. In contrast to inclusive DIS, jet production is not dominated by quark scattering, but also sensitive to gluon-initiated processes. At the same time, only cold nuclear effects are measured in (pointlike) electron-ion collisions in contrast to AA collisions and possibly even pA collisions, where collective effects are currently hotly debated [13]. Our calculations are based on previous work on jet production in photoproduction [14] and DIS [15] at next-to-leading order (NLO), which we have recently systematically improved in both cases to approximate next-to-next-to-leading order (aNNLO) [16,17] with a unified approach to soft and virtual corrections [18]. Note that very recently also full NNLO calculations of inclusive-jet [19] and dijet production [20] in DIS have become available, which show that the NNLO corrections are moderate in size, except at the kinematical edges, and that their inclusion leads to a substantial reduction of the scale variation uncertainty on the predictions. Where available, the full NNLO calculations confirm the aNNLO results even at surprisingly large distances from the hadronic threshold. We emphasize again that our focus here is not the impact of higher-order corrections in ep

[*]michael.klasen@uni-muenster.de
[†]karol.kovarik@uni-muenster.de
[‡]j_pott04@uni-muenster.de

 © 2017 American Physical Society

collisions, but rather the sensitivity of this process to nuclear effects in eA collisions at the EIC.

The remainder of this paper is organized as follows: In Sec. II, we describe our theoretical setup, including in particular our choices of renormalization and factorization scales and PDF sets. In Sec. III, we review the proposed experimental conditions for the two possible EIC designs and their detectors, i.e. BNL's proposal to add an electron ring to the existing Relativistic Heavy Ion Collider (eRHIC) and Jefferson Laboratory's proposal to build a medium energy electron-ion collider (MEIC) or Jefferson Laboratory EIC (JLEIC) using the upgraded 12 GeV Continuous Electron Beam Accelerator Facility (CEBAF). We base our assumptions on publicly available information from the EIC white paper [3] and updates shown at the POETIC 7 conference [21,22]. Our numerical results are presented in Sec. IV for a variety of EIC realizations and nuclei of different masses. Here, we also quantify the effect of higher-order corrections and, more importantly, estimate the impact of a future EIC on the reduction of nuclear PDF uncertainties. Our conclusions and an outlook to further studies are given in Sec. V.

II. JET PRODUCTION IN DIS AT APPROXIMATE NNLO OF QCD

The QCD factorization theorem allows us to write the differential cross section for inclusive-jet production on a nucleus A,

$$\mathrm{d}\sigma = \sum_a \int \mathrm{d}y f_{\gamma/e}(y) \int \mathrm{d}x f_{a/A}(x,\mu_F) \mathrm{d}\sigma_{\gamma a}(\alpha_s,\mu_R,\mu_F), \tag{2.1}$$

as a convolution of the photon-parton cross section $\mathrm{d}\sigma_{\gamma a}(\alpha_s,\mu_R,\mu_F)$ with the flux of virtual photons in the electron, $f_{\gamma/e}(y)$, and the PDFs of partons a in the nucleus A, $f_{a/A}(x,\mu_F)$. The fractional energy transfer of the electron in the nuclear rest frame is defined as $y = (p\cdot q)/(p\cdot k)$ with p and k the momenta of the incoming nucleus and electron, respectively, and q the momentum of the exchanged photon with $Q^2 = -q^2$. x is the longitudinal momentum fraction of the parton in the nucleus; μ_R and μ_F are the renormalization and factorization scales, respectively; and α_s is the strong coupling, in which the partonic cross section is perturbatively expanded.

For our NLO calculations, we employ the program `JetViP` [15,23], which we have recently improved to a NNLO [17] with a unified approach to soft and virtual corrections [18]. In this approach, the NLO corrections can be expressed in terms of a master formula,

$$\mathrm{d}\sigma_{\gamma a}^{\mathrm{NLO}} = \mathrm{d}\sigma_{\gamma a}^{\mathrm{LO}} \frac{\alpha_s(\mu_R)}{\pi} [c_3 D_1(z) + c_2 D_0(z) + c_1 \delta(1-z)], \tag{2.2}$$

which is ordered in terms of the leading and next-to-leading logarithms

$$D_l(z) = \left[\frac{\ln^l(1-z)}{1-z}\right]_+ \tag{2.3}$$

at partonic threshold ($z \to 1$) in pair-invariant-mass kinematics with $l \le 2n-1$ and $n = 1$ at NLO, $n = 2$ at NNLO etc. The NNLO master formula is given in Eq. (2.17) of Ref. [18], as are (in the section preceding this equation) the general formulas for the universal coefficients c_i. The process-dependent ingredients of the NNLO master formula were extracted from our explicit NLO calculation wherever possible [17].

In addition to the photon virtuality Q^2, inclusive-jet production depends on a second hard scale, the jet transverse momentum p_T. A customary choice of scales is therefore

$$\mu_R^2 = (Q^2 + p_T^2)/2 \quad \text{and} \quad \mu_F^2 = Q^2, \tag{2.4}$$

where the choice of μ_F is motivated by the fact that the same factorization scale can be used in the calculation of jet and inclusive DIS cross sections [24]. Jets are reconstructed in the Breit frame using the anti-k_T algorithm with a distance parameter $R = 1$ in the $\eta - \phi$ plane and a massless p_T recombination scheme [25]. Within experimental errors, consistent results were obtained with the k_T algorithm [26] by the H1 Collaboration at DESY HERA [24]. For the nuclear PDFs and their current uncertainties, we employ the nCTEQ15 fit with 32 error PDFs, and we estimate the impact of the inclusive pion production data from BNL RHIC with its nCTEQ15-np variant [6].

III. EXPERIMENTAL CONDITIONS AT AN ELECTRON ION COLLIDER

The experimental conditions at a future EIC depend on the selected site. At BNL, the existing RHIC is planned to continue accelerating nuclei to beam energies of up to $E_A = 100$ GeV per nucleon. It would have to be supplemented by a new electron beam with energy $E_e = 16$ to 21 GeV. The center-of-mass energy would then reach $\sqrt{s} = 80$ to 90 GeV and the integrated annual luminosity approximately 10 fb^{-1} for the lower energy and a third of that value for the higher energy [3].

At Jefferson Lab, the medium energy electron-ion collider (MEIC) would be based on the upgraded Continuous Electron Beam Accelerator Facility (CEBAF), which provides a high-luminosity electron beam of $E_e = 12$ GeV. It would have to be supplemented by an ion accelerator that could reach energies of $E_A = 40$ GeV per nucleon, leading to a lower center-of-mass energy of $\sqrt{s} = 45$ GeV, but a higher integrated annual luminosity of $\mathcal{L} = 100$ fb^{-1} [3].

Under all three of these conditions, the kinematic plane in x and Q^2 would be extended considerably, as can be seen in Fig. 1.5 of Ref. [3], i.e. from $x \ge 4\times 10^{-3}$ in νA DIS and

$x \geq 10^{-2}$ in $eA/\mu A$ DIS to values of $x \geq 10^{-4}$ and below in the Jefferson Laboratory and BNL designs, respectively, while simultaneously extending the range in Q^2 from 10^2 GeV^2 to 10^3 GeV^2 and beyond. In this way, the experimental information on the partonic structure of heavy nuclei would soon rival that of protons obtained at DESY HERA. In the following section, we will provide numerical results for each of the three accelerator designs mentioned above. Note that upgrade options exist for both sites, which may allow us to also reach beam energies of up to $E_A = 100$ GeV per nucleon with the Jefferson Laboratory EIC (JLEIC) [21] and annual luminosities of up to 100 fb^{-1} with eRHIC at BNL [22].

For both sites, similar detector requirements have been specified. They aim at a kinematic coverage of $Q^2 > 1$ GeV^2 and $0.01 \leq y \leq 0.95$ by using either the scattered electron or the hadronic final state with the Jacquet-Blondel method, which has proven advantageous at very low values of y at DESY HERA. The electromagnetic calorimeter would span the rapidity range $-4 < \eta < 4$ [3]. No specifications have so far been fixed for the hadronic calorimeter, so that we assume the same coverage. At DESY HERA, jets have been reconstructed in the Breit frame down to transverse momenta of $p_T \geq 4$ GeV [24], which we assume to be also possible at a future EIC.

IV. NUMERICAL RESULTS

We now turn to our numerical results for inclusive-jet production at the EIC. First, we investigate the dependence of various differential cross sections on the EIC beam energies. Next, we quantify the size of NLO and aNNLO corrections to the LO cross sections. Third, we study the dependence of the cross sections on the type of the colliding nucleus. Finally, our main results concern a demonstration of the current nuclear PDF uncertainty on the inclusive-jet cross sections and the impact that a future EIC might have on their reduction.

A. Inclusive-jet production at different EICs

In the following, we shall always display four typical differential cross sections for inclusive-jet production in DIS, i.e. the distributions in the jet transverse momentum p_T in the Breit frame and in the rapidity η in the lab frame, with the positive z-axis pointing in the direction of the ion beam, as well as the DIS variables Q^2 and Bjorken-x. These four differential cross sections are shown in Fig. 1 for e-Pb collisions and three different EIC designs: the RHIC ion beam with a nominal beam energy per nucleon of 100 GeV colliding with new electron beams of 16 GeV (full black lines) and 21 GeV (dotted green lines), respectively, and the CEBAF electron beam of 12 GeV energy colliding with a new ion beam of 40 GeV energy per nucleon (dashed blue lines).

At first sight, the p_T-range (top left) seems to be considerably larger in the eRHIC designs, where it extends to 35 GeV compared to only 15–20 GeV at the MEIC. The different nominal luminosities of 10 and 100 fb^{-1} lead, however, to a comparable number of about 100 events at 15 ± 0.5 GeV with only about 1 event surviving in a 20–30 GeV bin. For the detector acceptance, we have assumed that the hadronic calorimeter covers the rapidity range $-4 < \eta < 4$. The rapidity distribution in the lab frame (top right) shows, however, that the majority of the events is contained in the smaller range $-2 < \eta < 3$ at eRHIC and $-1.5 < \eta < 2$ at MEIC. Similarly to the case of inclusive DIS (cf. again Fig. 1.5 of Ref. [3]), the range in Q^2 would be extended in inclusive-jet production to 10^3 GeV^2 at MEIC and beyond at eRHIC (bottom left), while the range in Bjorken-x extends to 10^{-3} and below (bottom right). For this last distribution, which is perhaps the most interesting for the determination of nuclear PDFs, the advantage of the eRHIC designs with their considerably higher center-of-mass energies over the MEIC design is perhaps most notable. For all four distributions, the gain in reach from a 16 to a 21 GeV electron beam at eRHIC is, however, not very large and would probably be compensated by the loss in luminosity.

B. Inclusive-jet production at LO, NLO and aNNLO

Having established the experimental reaches in the relevant kinematic distributions, we now turn to the more theoretical aspect of the impact of higher-order corrections. Generally, the K-factors, i.e. the ratios of the NLO or aNNLO cross sections to those at LO, are not constant, but depend on the kinematic variables of the studied process, in particular those that set the perturbative scales entering the strong coupling and PDFs. Large corrections are expected at low scales and when the coupling or PDFs are large, and vice versa.

This expectation is clearly confirmed in Fig. 2, where we show the K-factors for the same four differential cross sections as before, but now only for one eRHIC design with a 16 GeV electron beam and a 100 GeV lead-ion beam. In the p_T distribution (upper left) and the Q^2 distribution (lower left), the NLO corrections reach a factor of 2–2.5 at low $p_T \geq 4$ GeV and $Q^2 \geq 1$ GeV^2. These are the two kinematic variables that enter the renormalization scale μ_R^2, while Q^2 alone sets the factorization scale μ_F^2; cf. Eq. (2.4). The corresponding cuts also set the scale in the rapidity distribution (upper right), where the K-factor rises above 2 at forward rapidities due to the high gluon density in this small-x regime. The same rise is therefore seen in the Bjorken-x distribution (lower right) at very low values of x. Since, for constant electron energy transfer, x scales directly with Q^2, the K-factors fall in both distributions towards higher values of these variables.

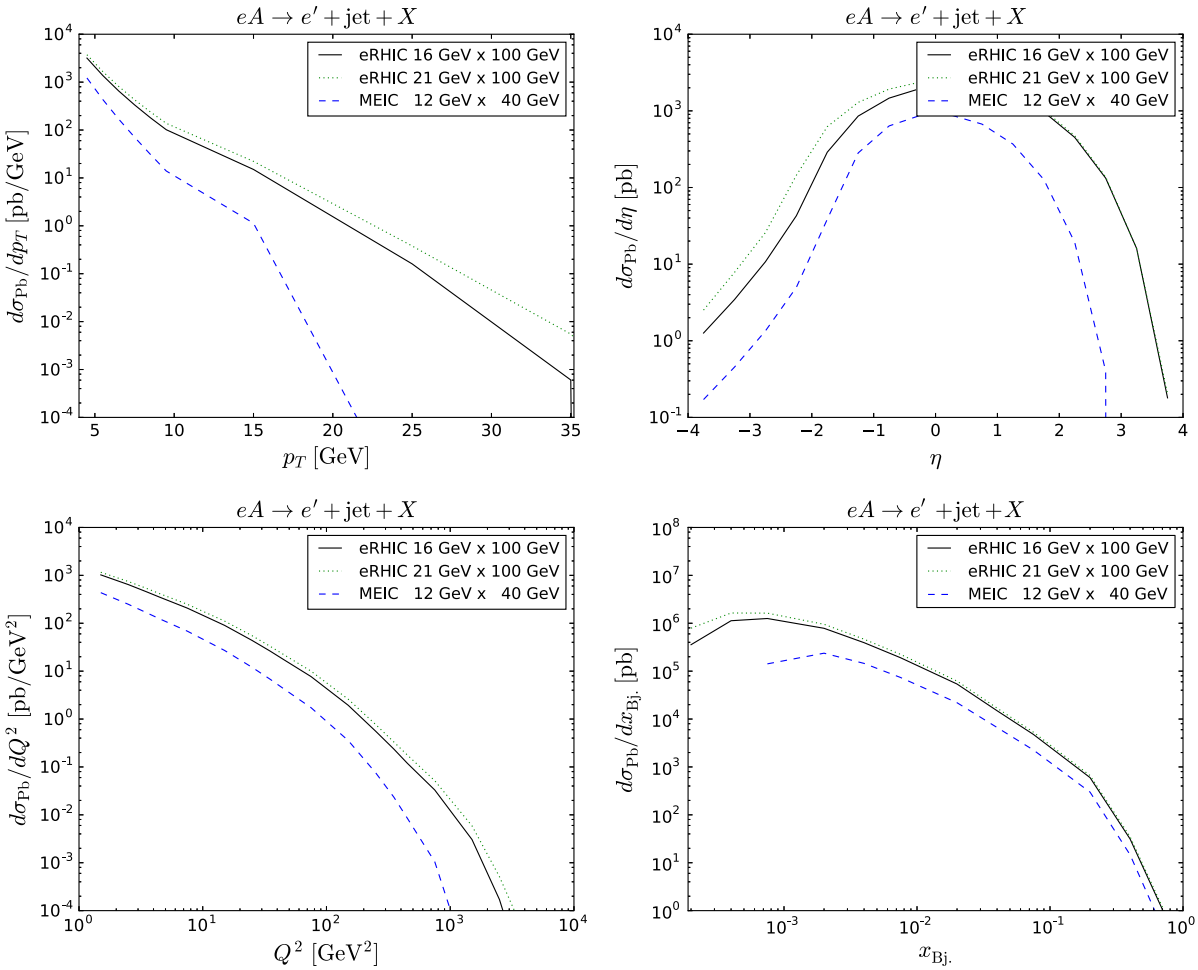

FIG. 1. Inclusive-jet production in electron–lead ion collisions at eRHIC and MEIC with electron beam energies of 12 to 21 GeV and ion beam energies per nucleon of 40 to 100 GeV. Shown are differential cross sections in the jet transverse momentum (top left), rapidity (top right), photon virtuality (bottom left) and Bjorken-x of the parton in the nucleus (bottom right).

Substantial K-factors (e.g. larger than 2) usually give rise to doubts about the stability of the perturbative calculation. Often, they can, however, be explained by the opening-up of additional partonic channels. Here, this is in particular the case for the splitting of low-x gluons into quark-antiquark pairs which then scatter off the virtual photon. In Fig. 2 the stability of the perturbative calculation is also established by the fact that the aNNLO K-factor (dotted-dashed red lines) corrections are very similar to those at NLO (full black lines). This confirms the observation in the exact NNLO calculations that the NNLO corrections are moderate in size, but lead to a stabilization of the cross sections with respect to variations of the renormalization and factorization scales (see above) [19,20].

C. Inclusive-jet production on different nuclei

The main goal of our work is to demonstrate the sensitivity of an EIC to nuclear PDF effects and to establish which regions (shadowing, antishadowing, EMC suppression, Fermi motion) could be constrained there. We therefore show in Fig. 3 ratios of nuclear over bare proton cross sections, differential in the same kinematic variables as before, for typical light and heavy nuclei: He-4 (dotted-dashed red lines), C-12 (dotted green lines), Fe-56 (dashed blue lines), and Pb-208 (full black lines). The EIC design is the same as before, i.e. an eRHIC machine with electron and ion beam energies (per nucleon) of 16 and 100 GeV, respectively.

Significant reductions of 20% and more are seen at large p_T and Q^2, very forward rapidities and both small and large values of x. The region of small $x < 10^{-3}$ with particularly high gluon and sea quark densities, corresponding to very forward rapidities, is known to be sensitive to nuclear shadowing induced by rescattering [27]. A particularly interesting model of nuclear shadowing is the leading-twist approach [28], which is based on the relationship between nuclear shadowing and diffraction on a nucleon and which can be tested, among other processes, in ultraperipheral collisions at the LHC [29,30]. The shadowing effect is known to decrease with the mass number of the nucleus

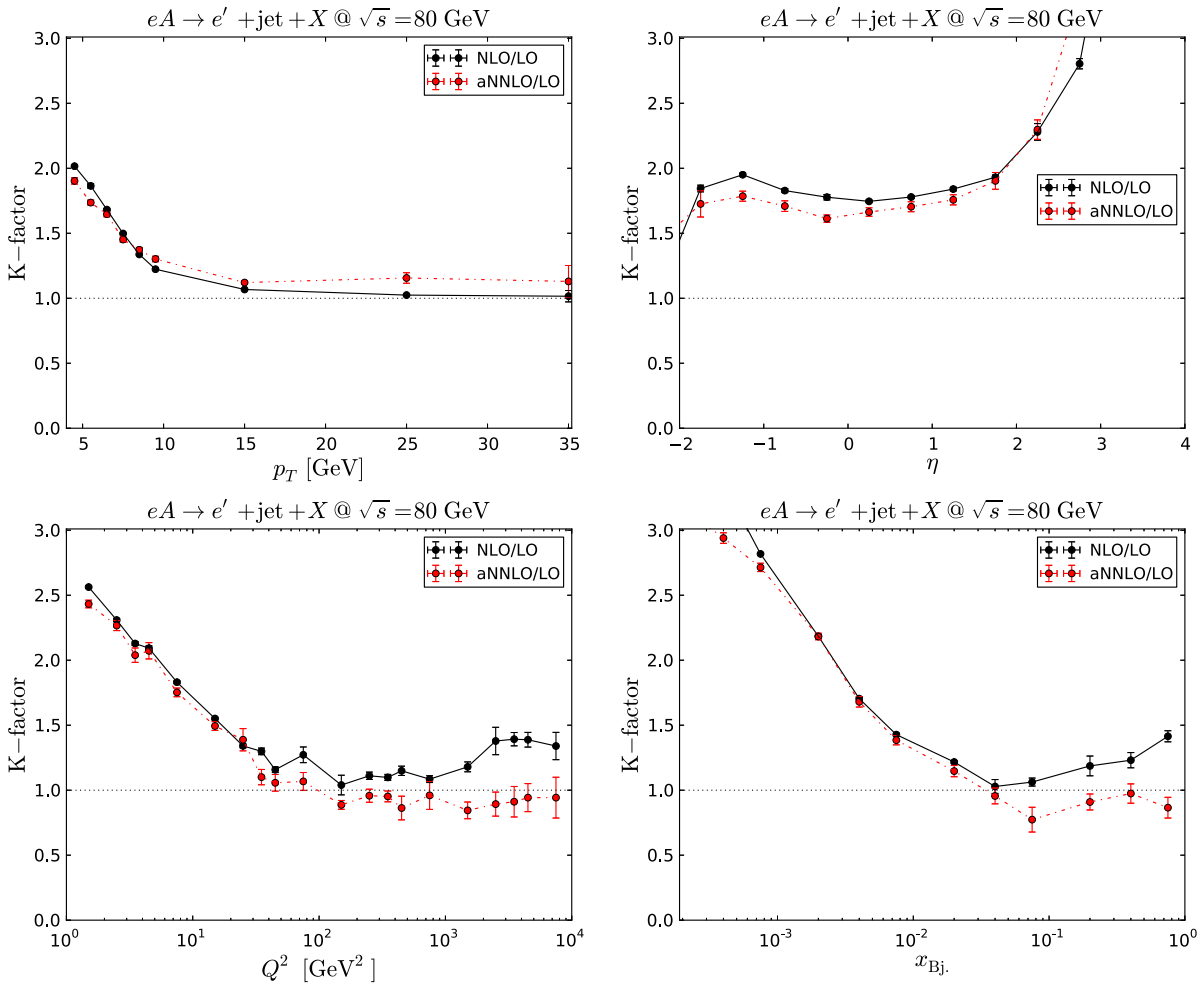

FIG. 2. Inclusive-jet production in electron–lead ion collisions with beam energies of 16 and 100 GeV, respectively, at eRHIC. Shown are the K-factors (ratios) of NLO/LO (full black lines) and aNNLO/LO (dotted-dashed red lines) cross sections as a function of the jet transverse momentum (top left), rapidity (top right), photon virtuality (bottom left) and Bjorken-x (bottom right). Error bars indicate the numerical integration accuracy.

[27], and this is also clearly observed in Fig. 3. From Pb-208 to Fe-56, C-12, and He-4, the effect is reduced from 22% to about 12, 6 and 3% at $x \simeq 2 \times 10^{-4}$, respectively.

Reductions of up to 35% are seen in the large-x regime of the EMC suppression, which is usually attributed to non-perturbative QCD effects on the valence quark distributions such as multiquark clusters, dynamical rescaling, or nuclear binding, but for which a theoretical consensus is still missing [31,32]. Also this reduction decreases with the nuclear mass number, although less rapidly, i.e. from 35% for Pb-208 and Fe-56 to 25% for C-12 and 20% for He-4.

Enhancements of up to 10% are observed at low p_T and low and medium Q^2 as well as central rapidities and intermediate values of $x \simeq 10^{-2}$. This so-called antishadowing region is not only required by momentum conservation, but can also be explained with constructive interference of multiple scattering amplitudes [33,34]. It thus is expected to be theoretically connected to the shadowing region, and the nuclear mass dependence is indeed very similar. Since the experimental uncertainty on determinations of nuclear PDFs at the EIC is expected to be dominated by a 2% systematic error (black error bars in Fig. 3), and not by statistics (cf. Fig. 3.25 of Ref. [3]), even effects of this size should be measurable at the EIC.

D. Sensitivity to nuclear parton density functions

The question is now what impact the EIC can have on a reduction of the nuclear PDF uncertainties compared to our current knowledge from fixed-target DIS and DY experiments. To this end, we show in Fig. 4 the same central predictions as in the previous section of the nCTEQ15 fit to these data for Pb-208 (full black lines), but supplement it now with the envelope of the corresponding set of 32 error PDFs (red bands) determined with the Hessian method [35,36]. The latter relies on the assumption that, near its

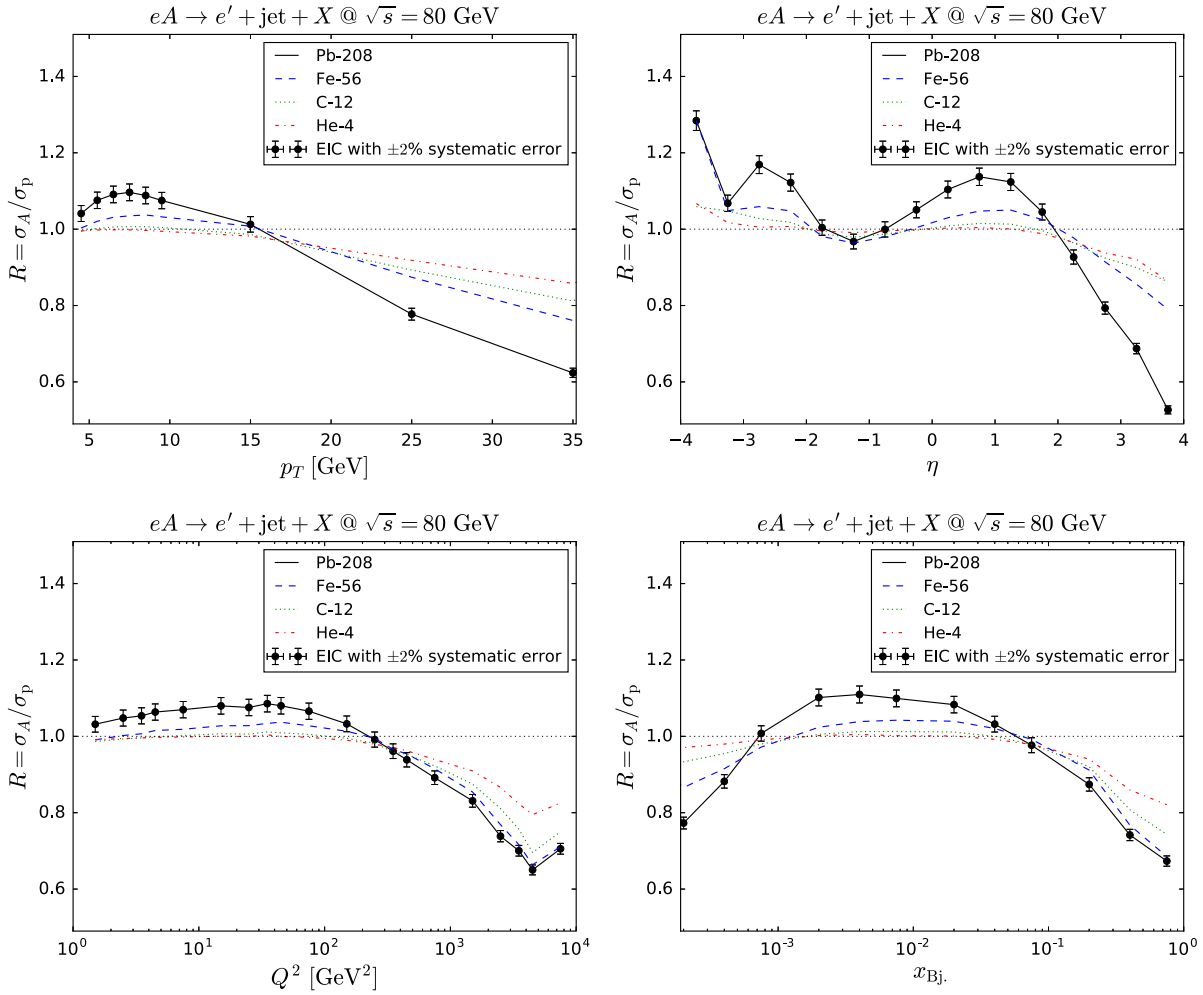

FIG. 3. Inclusive-jet production in electron-ion collisions with beam energies of 16 and 100 GeV, respectively, at eRHIC for different nuclei: Pb-208 (full black lines), Fe-56 (dashed blue lines), C-12 (dotted green lines), and He-4 (dotted-dashed red lines). Shown are the ratios of electron-ion over electron-proton cross sections as a function of the jet transverse momentum (top left), rapidity (top right), photon virtuality (bottom left) and Bjorken-x (bottom right). Error bars indicate the expected experimental precision.

minimum, the χ^2-function can be approximated by a quadratic form of the fitting parameters involving a matrix of second-order partial derivatives with respect to the parameter shifts from the minimum, which must then be diagonalized. We are particularly interested in the gluon contribution, which suffers from the largest uncertainties [6] and whose relative contribution to the differential cross sections is therefore shown in addition (dashed blue lines).

What we observe at large rapidities (top right) and even more at small values of x (bottom right) is that the gluon contributes substantially there (up to 70%) and that the nuclear PDF uncertainty reaches values of ±25%. In these regions, the EIC would therefore have the greatest impact and might eventually lead to a reduction of the uncertainty by an order of magnitude (black error bars). A similar reduction of the gluon uncertainty has been estimated to be possible in inclusive DIS and charm production at an EIC with 20 GeV electrons and 100 GeV gold ions [4] or at an LHeC [37]. The complementary regions, in particular the valence-quark-dominated region at medium-large x, have considerably smaller uncertainties of about ±10%, which would, however, still be reduced with an EIC by a factor of 5. If one integrates over the rapidity, as has been done in the p_T (top left) and Q^2 (bottom left) distributions, the uncertainty in the gluon-dominated regions at low values of p_T and Q^2 shrinks considerably, as one averages over large regions of x. At large p_T and Q^2, however, one probes also large values of x, which can be estimated by $x_T = 2p_T/\sqrt{s}$ and $Q^2/(sy)$, respectively. At very large x, information on nuclear PDFs is again very poor, as this region is difficult to reach in fixed-target collisions, so that the nuclear PDF uncertainty rises there to values of $+30/-10\%$.

In our last figure, Fig. 5, we repeat the same study as before, but include now also inclusive pion data from BNL RHIC in the nCTEQ15 estimate of the nuclear PDF uncertainty. As we mentioned before, this additional information depends on theoretical assumptions about the fragmentation function of quarks and gluons into pions.

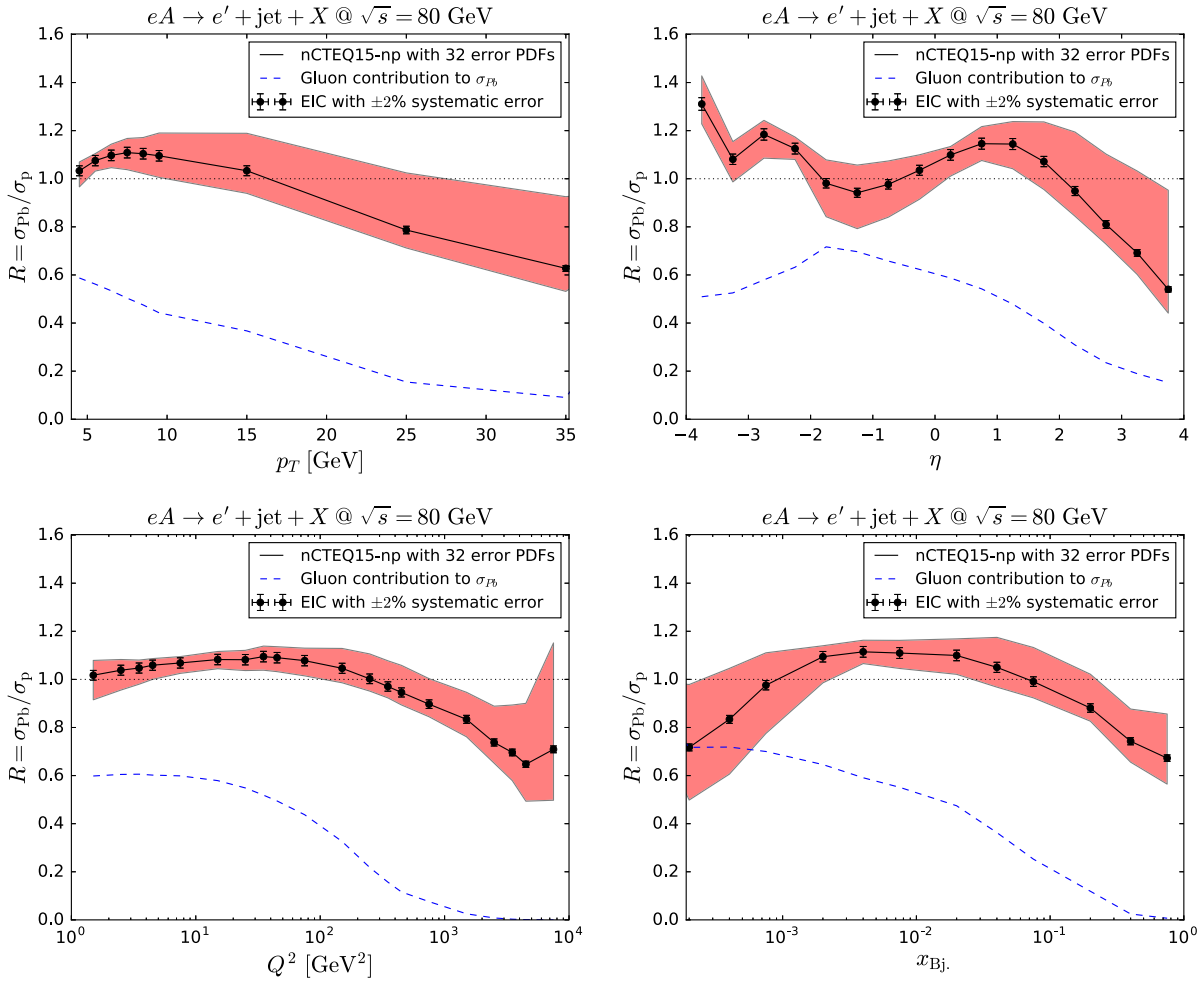

FIG. 4. Inclusive-jet production in electron–lead ion collisions with beam energies of 16 and 100 GeV, respectively, at eRHIC. Shown is the ratio of electron–lead ion over electron-proton cross sections (full black lines) including the current nuclear PDF uncertainty from the nCTEQ15 fit to DIS and DY data only (red bands) as well as the relative gluon contribution to the total cross section (dashed blue lines) as a function of the jet transverse momentum (top left), rapidity (top right), photon virtuality (bottom left) and Bjorken-x (bottom right). Error bars indicate the expected experimental precision.

Comparing Figs. 4 and 5 reveals that this additional information reduces the uncertainty by about a third, in particular at large rapidity and low Bjorken-x, but also at large p_T and Q^2, but that even under this additional assumption there is still large room for improvement from the EIC (black error bars).

It is interesting to confront the full nCTEQ15 fit using the inclusive pion data from D-Au collisions at BNL RHIC (solid black lines and red bands) with another, even more recent nPDF analysis, EPPS16 [7], which also includes these data, but in addition uses CERN LHC data on W and Z production and, more importantly, dijet production in p-Pb collisions at a center-of-mass energy of 5.02 TeV [38]. Therefore, in Fig. 5 the central EPPS16 predictions are also shown (dotted green lines), together with the envelope of the corresponding set of 40 error PDFs (green bands), determined again with the Hessian method. Overall, one observes that the shapes of the cross section ratios in the four distributions differ somewhat, in particular at the kinematic edges. While at low p_T (top left) nCTEQ15 and EPPS16 make very similar predictions, at high p_T EPPS16 predicts about half the suppression from nCTEQ15 with an uncertainty that is also about half as big. This is not surprising, as the fitted CMS dijet production data extend to jets of $p_T \simeq 40$ GeV [38], which is much higher than the $p_T < 16$ and 17 GeV pions that were measured with PHENIX [39] and STAR [40] at BNL RHIC, respectively. Similarly, EPPS16 fitted to CMS dijet data with rapidities up to $\eta < 2.5$, while the pion measurements by PHENIX and STAR extended only to $|\eta| \leq 0.35$ and $0 < \eta < 1$, respectively, so that differences at very forward rapidities are to be expected (top right). The reduced uncertainty there translates into a similarly reduced uncertainty at low Bjorken-x (bottom right), while in the Q^2 distribution the nCTEQ15 and EPPS16 predictions are again very similar, except at very high scales (bottom left). Under the assumption that jets are not modified (or at least modified less than pions) in pA collisions, the EPPS16

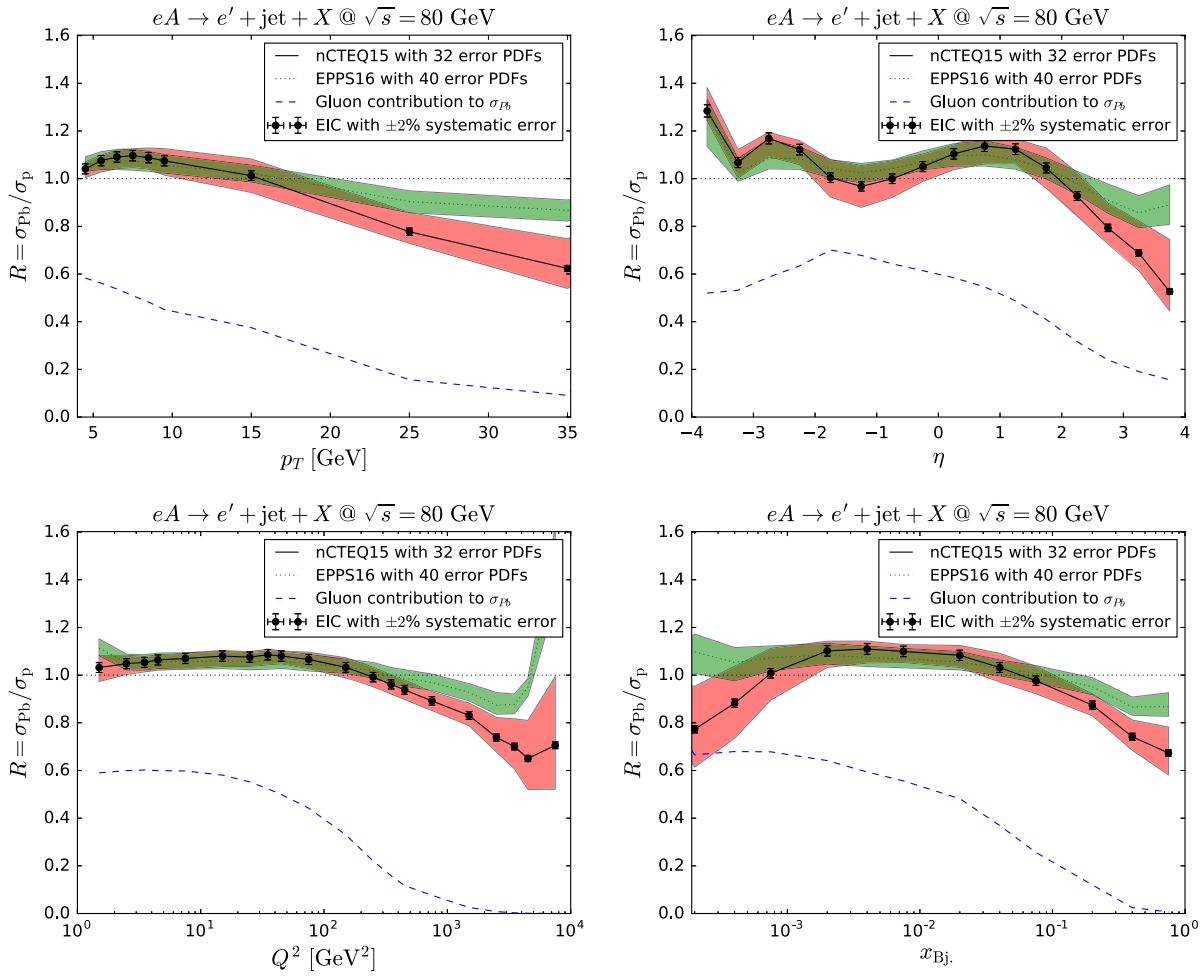

FIG. 5. Same as Fig. 4 for the nCTEQ15 fit including also inclusive pion data from D-Au collisions at BNL RHIC, and for the central EPPS16 fit (dotted green lines) to—in particular—dijet data from the LHC as well as the corresponding (green) error bands.

predictions are already quite precise, but would still be improved at an EIC by a factor of up to 5.

V. CONCLUSION AND OUTLOOK

Let us therefore now come to our conclusions. In this paper, we have made predictions for inclusive-jet production in electron-ion collisions at a possible future EIC. Our goal was in particular to establish the benefit that such a collider might have on a more precise determination of nuclear PDFs, which is not only required to enhance our knowledge of quark and gluon dynamics in the nucleus, but also to allow for a reliable extraction of hot nuclear matter properties after a proper subtraction of cold nuclear effects. Theoretically, our calculations were based on a full NLO and an approximate NNLO calculation, implemented in the program `JetViP`. While the NLO corrections were large, in particular at low perturbative scales, perturbative stability was restored at aNNLO in line with expectations from full NNLO calculations. Phenomenologically, we have established that measurements of inclusive-jet production at an EIC would extend the kinematic ranges to $Q^2 \leq 10^3$ GeV^2 and $x \geq 10^{-4}$ similarly to inclusive DIS and allow us to reduce the uncertainty on nuclear PDFs, in particular the one of the gluon at low x, by factors of 5 to 10. This improvement would probably not be possible in inclusive DIS alone, but would alternatively require additional charm tagging possibilities.

Future calculations could properly include jet mass effects in the aNNLO calculation [41] (although as we have seen the impact of these corrections is small) and extend the present study to dijet production, which would allow for more complete kinematic constraints. More differential studies of single, two and three jets and their shapes at the EIC might help to establish if they are modified in eA collisions compared to ep collisions, similarly to the modification of the pion fragmentation function in AA collisions and possible collective effects in pA collisions. It would then become possible to investigate transport properties of the cold nuclear medium and test the strong gluon field paradigm [42]. Finally, even transverse-momentum-dependent distribution functions (TMDs) of gluons in protons and nuclei might become accessible in

measurements of dijet asymmetries in polarized or unpolarized ep and eA collisions [43].

ACKNOWLEDGMENTS

We thank the organizers of the 7th International Conference on *Physics Opportunities at an ElecTron-Ion-Collider* (POETIC 7), which motivated this study, for the kind invitation and C. Klein-Bösing for useful discussions. This work has been supported by the Bundesministerium für Bildung und Forschung (BMBF) under Contract No. 05H15PMCCA. All figures have been produced using `Matplotlib` [44].

[1] J. C. Collins, D. E. Soper, and G. F. Sterman, Adv. Ser. Dir. High Energy Phys. **5**, 1 (1989).
[2] J. Butterworth *et al.*, J. Phys. G **43**, 023001 (2016).
[3] A. Accardi *et al.*, Eur. Phys. J. A **52**, 268 (2016).
[4] N. Armesto, in *7th International Conference on Physics Opportunities at an ElecTron-Ion-Collider (POETIC 7), Philadelphia, Nov. 14, 2016*, https://indico.bnl.gov/getFile.py/access?contribId=54&sessionId=1&resId=0&materialId=slides&confId=2095.
[5] D. de Florian, R. Sassot, P. Zurita, and M. Stratmann, Phys. Rev. D **85**, 074028 (2012).
[6] K. Kovarik *et al.*, Phys. Rev. D **93**, 085037 (2016).
[7] K. J. Eskola, H. Paukkunen, and C. A. Salgado, J. High Energy Phys. 04 (2009) 065; K. J. Eskola, P. Paakkinen, H. Paukkunen, and C. A. Salgado, Eur. Phys. J. C **77**, 163 (2017).
[8] N. Armesto, H. Paukkunen, J. M. Penn, C. A. Salgado, and P. Zurita, Eur. Phys. J. C **76**, 218 (2016).
[9] M. Hirai, S. Kumano, and T.-H. Nagai, Phys. Rev. C **76**, 065207 (2007); M. Hirai, J. Phys. Soc. Jpn. Conf. Proc. **12**, 010024 (2016).
[10] I. Schienbein, J. Y. Yu, K. Kovarik, C. Keppel, J. G. Morfin, F. Olness, and J. F. Owens, Phys. Rev. D **80**, 094004 (2009).
[11] M. Klasen and M. Brandt, Phys. Rev. D **88**, 054002 (2013); M. Brandt, M. Klasen, and F. König, Nucl. Phys. **A927**, 78 (2014).
[12] A. Kusina *et al.*, arXiv:1610.02925.
[13] B. Abelev *et al.* (ALICE Collaboration), Phys. Lett. B **719**, 29 (2013); B. B. Abelev *et al.* (ALICE Collaboration), Phys. Lett. B **726**, 164 (2013); B. B. Abelev *et al.* (ALICE Collaboration), Phys. Rev. C **90**, 054901 (2014).
[14] M. Klasen and G. Kramer, Z. Phys. C **72**, 107 (1996); M. Klasen and G. Kramer, Z. Phys. C **76**, 67 (1997); M. Klasen, T. Kleinwort, and G. Kramer, Eur. Phys. J. direct C **1**, 1 (2000).
[15] M. Klasen, G. Kramer, and B. Pötter, Eur. Phys. J. C **1**, 261 (1998).
[16] M. Klasen, G. Kramer, and M. Michael, Phys. Rev. D **89**, 074032 (2014).
[17] T. Biekötter, M. Klasen, and G. Kramer, Phys. Rev. D **92**, 074037 (2015).
[18] N. Kidonakis, Int. J. Mod. Phys. A **A19**, 1793 (2004).
[19] G. Abelof, R. Boughezal, X. Liu, and F. Petriello, Phys. Lett. B **763**, 52 (2016).
[20] J. Currie, T. Gehrmann, and J. Niehues, Phys. Rev. Lett. **117**, 042001 (2016).
[21] R. Yoshida, *7th International Conference on Physics Opportunities at an ElecTron-Ion-Collider (POETIC 7), Philadelphia, 2016*, https://indico.bnl.gov/getFile.py/access?contribId=62&sessionId=4&resId=0&materialId=slides&confId=2095.
[22] B. Müller, *7th International Conference on Physics Opportunities at an ElecTron-Ion-Collider (POETIC 7), Philadelphia, 2016*, https://indico.bnl.gov/getFile.py/access?contribId=61&sessionId=4&resId=0&materialId=slides&confId=2095.
[23] B. Pötter, Comput. Phys. Commun. **133**, 105 (2000).
[24] V. Andreev *et al.* (H1 Collaboration), Eur. Phys. J. C **75**, 65 (2015).
[25] M. Cacciari, G. P. Salam, and G. Soyez, J. High Energy Phys. 04 (2008) 063.
[26] S. D. Ellis and D. E. Soper, Phys. Rev. D **48**, 3160 (1993).
[27] N. Armesto, J. Phys. G **32**, R367 (2006).
[28] L. Frankfurt, V. Guzey, and M. Strikman, Phys. Rev. D **71**, 054001 (2005).
[29] A. J. Baltz *et al.*, Phys. Rep. **458**, 1 (2008).
[30] V. Guzey and M. Klasen, J. High Energy Phys. 04 (2016) 158.
[31] M. Arneodo, Phys. Rep. **240**, 301 (1994).
[32] D. F. Geesaman, K. Saito, and A. W. Thomas, Annu. Rev. Nucl. Part. Sci. **45**, 337 (1995).
[33] S. J. Brodsky, I. Schmidt, and J. J. Yang, Phys. Rev. D **70**, 116003 (2004).
[34] L. Frankfurt, V. Guzey, and M. Strikman, arXiv:1612.08273.
[35] J. Pumplin, D. R. Stump, and W. K. Tung, Phys. Rev. D **65**, 014011 (2001).
[36] J. Pumplin, D. Stump, R. Brock, D. Casey, J. Huston, J. Kalk, H. L. Lai, and W. K. Tung, Phys. Rev. D **65**, 014013 (2001).
[37] I. Helenius, H. Paukkunen, and N. Armesto, *Proc. Sci.*, DIS2016 (2016) 276 [arXiv:1606.09003].
[38] S. Chatrchyan *et al.* (CMS Collaboration), Eur. Phys. J. C **74**, 2951 (2014).
[39] S. S. Adler *et al.* (PHENIX Collaboration), Phys. Rev. Lett. **98**, 172302 (2007).
[40] B. I. Abelev *et al.* (STAR Collaboration), Phys. Rev. C **81**, 064904 (2010).
[41] D. de Florian, P. Hinderer, A. Mukherjee, F. Ringer, and W. Vogelsang, Phys. Rev. Lett. **112**, 082001 (2014).
[42] I. Vitev, in *7th International Conference on Physics Opportunities at an ElecTron-Ion-Collider (POETIC 7), Philadelphia, 2016*, https://indico.bnl.gov/getFile.py/access?contribId=77&sessionId=9&resId=0&materialId=slides&confId=2095.
[43] D. Boer, P. J. Mulders, C. Pisano, and J. Zhou, J. High Energy Phys. 08 (2016) 001.
[44] J. D. Hunter, Comput. Sci. Eng. **9**, 90 (2007).